Surface Chemistry of Rh–Mo/γ-Al₂O₃: An Analysis of Surface Acidity

Eric E. Lowenthal, Stephan Schwarz,[1] and Henry C. Foley[2]

Center for Catalytic Science and Technology, Department of Chemical Engineering, University of Delaware, Newark, Delaware 19716

This study highlights the nature of the interactions between the transition metals in the Rh–Mo/γ-Al₂O₃ system and the underlying alumina surface. The investigation was carried out in the context of exploring the retrograde dehydration to dimethyl ether of primary alcohols produced at active metal sites during CO hydrogenation. Both native γ-Al₂O₃ and Rh–Mo/γ-Al₂O₃ samples were doped with KNO₃ in an attempt to create an alkaline–metal oxide layer on the support surface which would screen alcohols from underlying Lewis acidity. The samples were characterized by microreactor-based methanol dehydration studies, analysis of infrared spectra of adsorbed pyridine, and ammonia saturation and temperature-programmed desorption. As expected, the dehydration activity of the samples was strongly correlated to their potassium loading and, hence, their Lewis acidity. More intriguing, however, are the insights gained in this analysis concerning the nature of the interactions between Mo, Rh, and the Lewis acid sites on the alumina surface. Our results are consistent with the principle, suggested in the Mo/γ-Al₂O₃ literature, that our Mo(CO)₆ precursor interacts primarily with nonacidic hydroxyl groups on the dehydrated alumina surface. Furthermore, we provide strong evidence for the diminution of acidity brought on by the adsorption of Rh on Lewis acid sites of Mo/γ-Al₂O₃. © 1995 Academic Press, Inc.

INTRODUCTION

Past investigations of a series of alumina-supported bimetallic combinations of Group VI and noble transition metals identified synergistic characteristics of Rh–Mo/γ-Al₂O₃ (1, 2). Promoting rhodium with molybdenum oxide produced a catalyst with a significantly higher propensity for the production of oxygenates in the hydrogenation of CO than could be achieved using a monometallic rhodium catalyst at both atmospheric and moderate (~1.7 MPa) pressures. Other researchers have reported oxoselectivity and activity enhancements on silica- and alu-

mina-supported rhodium catalysts as a consequence of molybdenum promotion (3–6). Based on a combination of microreactor testing for CO hydrogenation, transmission electron microscopy (TEM) and XPS analysis, and H₂-chemisorption measurements, a qualitative model for the behavior of Rh in the presence of MoOₓ was proposed wherein the oxidized Mo acts primarily as a textural promoter in small, bimetallic crystallites (~0.5 nm), site-isolating rhodium aggregates which would otherwise tend to sinter and agglomerate at comparable loadings. These site-isolated rhodium aggregates are thought to be primarily responsible for the oxygenate chemistry of the catalyst in the presence of synthesis gas. Larger, rhodium-rich bimetallic aggregates (~1.0 to 1.5 nm) were proposed to be primarily responsible for the dissociative adsorption of CO and subsequent hydrocardon formation. Some infrared (IR) spectroscopic evidence in the literature (7, 8) points to the partial oxidation of larger rhodium particles via migration of molybdenum oxide onto the surface of such lager rhodium aggregates. Kip *et al.* (3), in an extended study of promoted Rh/SiO₂, employing temperature-programmed reduction and oxidation, transmission electron microscopy, and CO hydrogenation probe reactions, as well as infrared spectroscopic analysis, found evidence for molybdenum oxide migration onto rhodium aggregates (as opposed to the lack of migration demonstrated by oxides of thorium). More recently, in a study of Rh–Mo/SiO₂ derived from metal-carbonyl precursors, Trunschke *et al.* (6) suggest a textural promotion role for molybdenum oxide, wherein it stabilizes smaller rhodium aggregates—identified by their signature gem–dicarbonyl infrared doublets—against sintering and agglomeration upon exposure to reaction conditions.

Upon testing the Rh–Mo/γ-Al₂O₃ catalysts at industrially relevant pressures, the oxygenated components of the product slate from CO hydrogenation shifted from predominantly methanol (MeOH), at atmospheric pressure, to predominantly dimethyl ether (DME) and ethanol (EtOH), at moderate pressures. We have ascribed the tendency to dehydrate primary alcohol products to sec-

ondary ether products to acidic features of the catalysts based on mechanistic evidence in the literature (9–13). For example, Parera and Figoli (10) suggest the straightforward mechanism detailed in Fig. 1, wherein MeOH encounters a Lewis acid site on native alumina and dissociatively adsorbs onto the site, ejecting an H⁺ ion onto an adjacent basic oxygen atom. The surface species can then recombine to form the etherification products CH_3OCH_3 and H_2O. The chemistry governing (1) of Fig. 1 has been disputed in the literature (12, 13). Notably, using ¹⁸O-labeled alcohols, Decanio et al. (13) have demonstrated that the basic oxygen in a Lewis acid–base pair can cleave the carbon–oxygen bond in the alcohol in contrast to the electrophilic attack of the alcohol function by the Lewis site. While this reaction was detected using $CH_3^{18}OH$, the propensity of the surface toward basic attack was found to be a function of alkyl chain length. The net products in (1) are the same in either case. Hence, for the purposes of this study we have focused our characterization efforts on measuring Lewis acidity.

In this study, we quantify and manipulate the Lewis acidity of γ-Al₂O₃ and Rh-Mo/γ-Al₂O₃ in order to obtain insight into alcohol etherification over the Rh–Mo catalysts during hydrogenation of CO and, more importantly, the bimetallic interactions of the Rh and Mo with the alumina surface and their effect upon the acidity of the underlying support. To study the influence of surface acidity, we have synthesized a series of potassium-promoted catalysts from both native and transition-metal-loaded starting materials. The catalytic materials were then characterized using the following techniques: (i) evaluation of microreactor results for the direct dehydration of MeOH, (ii) analysis of IR spectra of adsorbed pyridine, and (iii) analysis of ammonia saturation and temperature-programmed desorption (TPD) spectra. By mapping the surface acidity of the various transition-metal-loaded samples, intriguing evidence concerning the nature of the interaction between the transition-metal precursors and the acidic surface features of the support became apparent. The implications of this evidence on the process by which transition-metal carbonyl precursors interact with the surface of alumina during chemisorption and calcination are also discussed herein.

METHODS

Catalyst Synthesis

The support common to all the samples tested in this study was γ-Al₂O₃ (American Cyanamid, BET surface area = 250 m²/g). In all cases, the support was dehydrated in air at atmospheric pressure and 120°C overnight for approximately 12 h prior to modification or testing. The samples synthesized in this study can be broadly divided into two categories: (i) doped, native alumina and (ii) doped Rh-Mo/γ-Al₂O₃.

Native alumina was doped with KNO₃ (EM Science) via either ion exchange or aqueous impregnation. In the
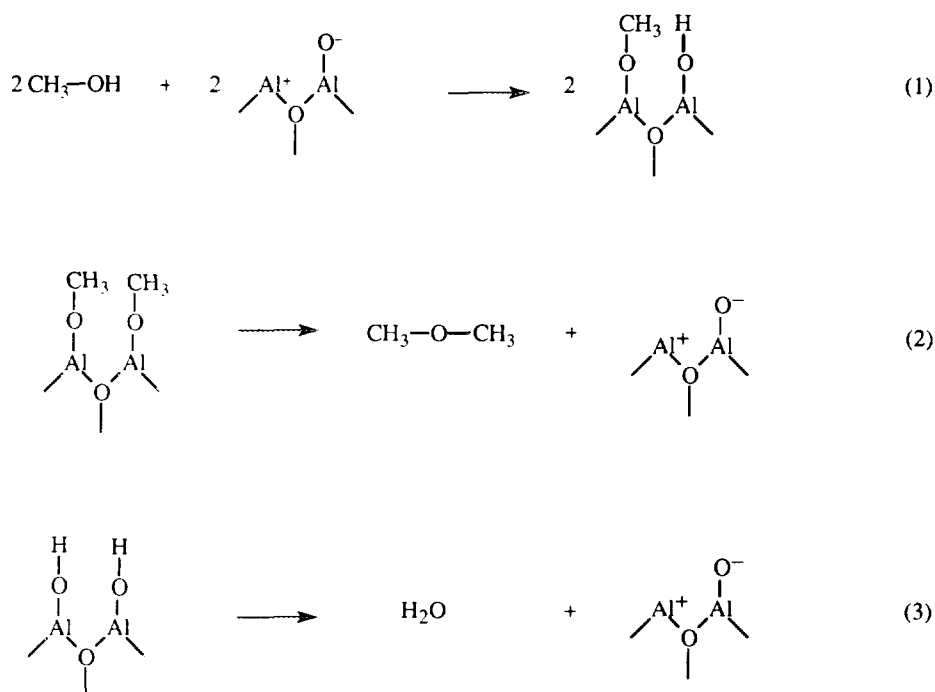

FIG. 1. Methanol dehydration mechanism on alumina, adapted from Ref. (10).

ion-exchange protocol, the dehydrated alumina was slurried and continuously stirred for 12 h in an aqueous solution of KNO_3. In the aqueous-impregnation protocol, the dehydrated alumina was impregnated with an aqueous solution of KNO_3 to incipient wetness (0.79 ml/g). In both methods, the doping step was followed by calcination in air at 300°C overnight for approximately 12 h. One of the aqueous impregnation samples was reimpregnated and calcined a second time to achieve a higher potassium loading. The second impregnation was necessary due to the solubility limit of KNO_3 and the pore volume capacity of the alumina.

In order to prepare potassium-doped Rh–Mo/γ-Al_2O_3 samples, transition-metal-loaded samples were first synthesized. Sixty grams of dehydrated alumina was slurried with 250 ml of anhydrous heptane (99+% pure, Aldrich). Following a refluxing step to degas the slurry, 11.0 g of $Mo(CO)_6$ (Strem) was added. After the chemisorption of the $Mo(CO)_6$ was complete, the resultant solid was filtered and placed in a fresh heptane slurry, and 5.0 g of $RH(I)(CO)_2(acac)$ (Strem) was added. The refluxing slurry was maintained throughout the synthesis under flowing N_2 (dried and deoxygenated) to prevent the precipitation of the transition-metal carbonyls as bulk metal oxides. The extent of chemisorption of the carbonyl precursors was monitored by (i) observation of color changes of the solid and of the supernatant in the slurry and (ii) IR analysis of both self-supporting wafers of the intermediate and final materials and IR analysis of samples of the supernatant to establish the complete conversion of carbonyls in the liquid phase. The final bimetallic catalyst was filtered and dried in air and was mildly calcined at 120°C overnight for approximately 12 h. A more detailed description of the synthesis protocol used to prepared related bimetallic samples was presented in an earlier publication (1).

Both the ion exchange and the aqueous impregnation methods described for the doping of alumina (vide supra) were explored to synthesize potassium-promoted Rh–Mo/γ-Al_2O_3 samples. Interestingly, however, the ultimately achievable potassium loading for the ion-exchanged Rh–Mo/γ-Al_2O_3 was considerably lower than that achieved on doped, native alumina.

Methanol Dehydration Studies

The catalytic materials synthesized in this study have been tested for their propensity to dehydrate MeOH. In the MeOH dehydration experiments, approximately 0.15 g of sample was packed into a 5-mm-i.d. Pyrex microreactor tube and loaded into a tube furnace (Lindberg 55031). The MeOH was fed to the packed bed by passing 25 cm^3/min of He carrier gas through a MeOH sparger, maintained at a constant temperature of 10°C with a cir-

culating temperature bath. The packed bed temperature was maintained at 180 to 250°C depending on the particular sample and objectives of the reactor test. The reactor effluent was separated and analyzed by gas chromotography using a 12-ft, 1/8-in-o.d. packed column containing 80 × 100 mesh Poropak T (Supelco) and a flame ionization detector to obtain conversion of MeOH to DME (or in the case of the Rh–Mo/γ-Al_2O_3 series of samples, DME, light hydrocarbons, and formaldehyde). All rate data reported in this study are for conversions of less than 10% so that differential reactor conditions can be assumed.

Pyridine Adsorption and IR Analysis

The pyridine (99+% pure C_5H_5N, Aldrich) used in this study was refluxed over excess CaH_2 for 48 h under flowing N_2 and distilled and stored on 5 Å molecular sieves prior to use in the surface characterization of catalyst samples. The dried pyridine was also degassed by repeated freeze–pump–thaw cycles before dosing the surface of a sample. The sample was ground to roughly 200 × 325 mesh (~60 μm) and pressed into a self-supporting wafer approximately 1.5 cm in diameter. The wafer was placed in a sealed quartz transmission infrared cell equipped with NaCl windows and two vacuum stopcocks for gas treatment and evacuation. The cell was then heated to 300°C and simultaneously evacuated to approximately 3 × 10^{-3} Torr (1 Torr = 133.3 Pa) until the IR peaks associated with water on the wafer surface and CO_2 in the purged chamber surrounding the cell had diminished to insignficant levels. Following dehydration to 300°C, the cell was cooled to 200°C. An IR background spectrum was then collected, and all other spectra collected from the sample were referenced to this background (i.e., evacuated sample at 200°C). Next, saturated pyridine vapor was allowed to equilibrate with the sample surface until repeated collection of IR spectra showed no increase in pyridine peak intensities (approximately 30 min). Finally, two sets of IR spectra were collected on the pyridine-saturated samples: (i) spectra for the samples in equilibrium with the saturated vapor and (ii) spectra for the surface after the wafers had been evacuated to 3 × 10^{-3} Torr, following dosing. All spectra discussed herein were recorded after 30 scans, have a resolution of 4 cm^{-1}, and were collected on a Nicolet 510 M fourier transform Infrared spectrometer.

Ammonia Saturation and Temperature-Programmed Desorption

As an additional measure of surface acidity, we collected ammonia saturation data and TPD spectra for the samples in Table 1. The ammonia used in the saturation and TPD analysis was 3.1 vol.% NH_3 in a balance of He

TABLE 1

Ammonia Saturation Measurements Reflecting
Surface "Acid Amount"

Sample	Reversible[a] NH₃ adsorption (μ moles/g sample)	Total NH₃ adsorption (μ moles/g sample)
γ-Al₂O₃ (American Cyanimid)	594 ± 58	2450 ± 66
8.2% K on γ-Al₂O₃	374 ± 37	2270 ± 75
11.9% K on γ-Al₂O₃	349 ± 33	3080 ± 133
2.5% Mo on γ-Al₂O₃	726 ± 71	2820 ± 83
2.8% Rh–3.4% Mo on γ-Al₂O₃	764 ± 71	2850 ± 75
2.8% Rh–3.4% Mo on γ-Al₂O₃; 0.03% K[b]	722 ± 66	2570 ± 62
2.8% Rh–3.4% Mo on γ-Al₂O₃; 0.08% K[b]	747 ± 71	2760 ± 75

[a] Reversible sites are defined as those NH₃-sensitive acid sites which desorb NH₃ upon heating to 400°C.

[b] The 2.8% Rh–3.4% Mo on γ-Al₂O₃ sample was used as the starting material for these potassium-doped catalysts. While elemental analysis was used to determine the potassium content, no analysis of transition metal content was conducted following the ion-exchange protocol.

(certified, Matheson). Approximately 0.3 g of 60 × 100 mesh (~200 μm) catalyst was packed in a 9-mm-i.d. quartz microreactor tube between plugs of glass wool, and the tube was placed in a tube furnace (Lindberg 55035) and put on-line with flowing He at 10 cm³/min. The sample was allowed to equilibrate at 50°C and was then dehydrated by ramping to 400°C at a rate of 7°C/min and soaking at 400°C for 50 min under flowing He. Finally, the sample was cooled to 50°C, the carrier gas stream was switched from He to NH₃ in He, and the gas eluted from the column was monitored with a thermal conductivity detector (TCD, Gow-Mac 40-250/252). When the baseline of the chromatogram had shifted and leveled off, indicating that the column was saturated with ammonia, the carrier was switched back to pure He and the column temperature was ramped from 50 to 400°C at 7°C/min and then soaked for 50 min at 400°C. The temperature program naturally led to the desorption of the NH₃, and this was manifest as a series of peaks in the chromatogram.

RESULTS

K-Doped γ-Al₂O₃

Our results support the contention that the tendency of alumina to dehydrate MeOH is inhibited with increasing potassium loading. Figure 2 depicts the steady-state rate of DME formation from MeOH as a function of potas-

sium loading on γ-Al₂O₃. The downward sloping trend in the data indicates that as the potassium loading increases, the tendency to dehydrate MeOH diminishes. The data shown for 8.2 and 11.9% potassium loadings resulted from samples made by the aqueous impregnation method.

The chemisorptive characterization data for this series of samples suggests that the decrease in methanol dehydration propensity with increasing potassium loading is due to a decrease in the surface acidity of the samples. From the IR analysis of Parry (14) for pyridine adsorbed on alumina, an intense peak at 1453 cm⁻¹, a strong peak at 1495 cm⁻¹, and a peak falling between 1600 and 1633 cm⁻¹ can be assigned to vibrational modes of pyridine coordinatively bonded to the Lewis acid sites of the surface. Parry's analysis also suggests that a broad band between 1580 and 1600 cm⁻¹ and a less intense peak at approximately 1435 cm⁻¹ are attributable to the vibrational modes of pyridine molecules physisorbed on the surface through hydrogen bonding or other dispersion forces. While the IR spectral pairs for each of the three samples (0, 8.2, and 11.9% K-doped γ-Al₂O₃) presented in Fig. 3 reflect the presence of Lewis acid sites, as well as physisorbed pyridine, the intensity of the chemisorptive peaks diminishes with increasing potassium loading. This attenuation of the chemisorptive peaks (1453, 1495, and 1600–1633 cm⁻¹) reflects a decrease in the strength or number of Lewis acid sites which coordinatively bond to the pyridine. By 11.9% K (Fig. 3C, after evacuation), the chemisorptive bands are absent; i.e., the acidity has been effectively suppressed. Note that the hydrogen-bonded shoulder at 1435 cm⁻¹ in the native alumina spectrum gives rise to the splitting of the convoluted band from ~1410 to 1460 cm⁻¹ for the spectra in equilibrium with the pyridine vapor as the potassium loading is increased.

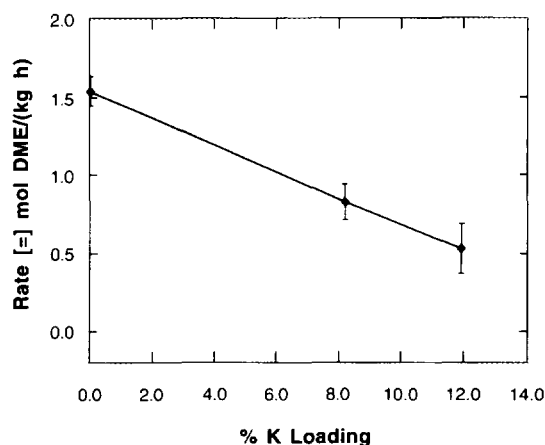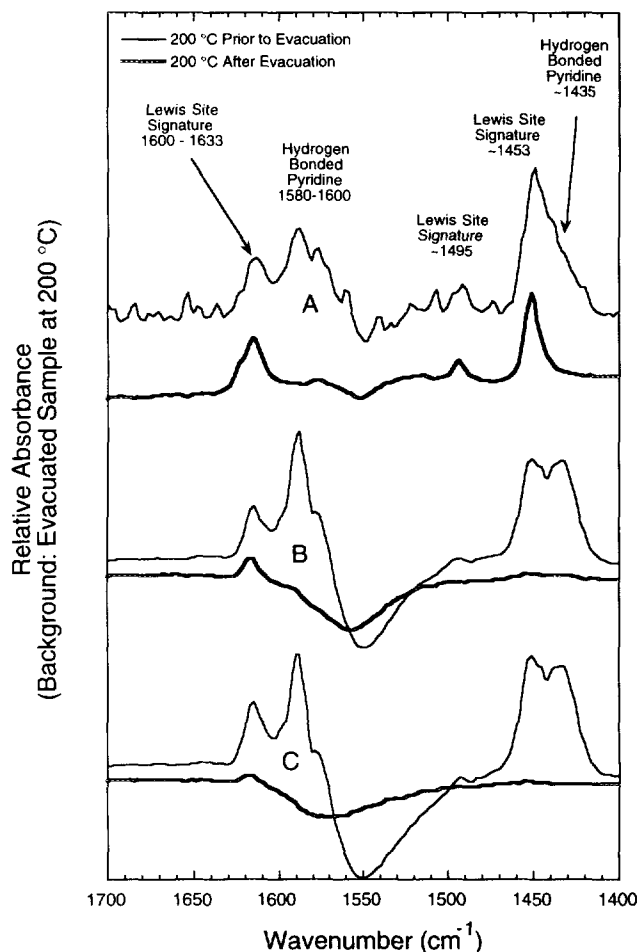FIG. 2. Steady-state rate of dimethyl ether formation as a function of potassium loading on γ-Al₂O₃.

FIG. 3. IR spectra of adsorbed pyridine. (A) Native γ-Al₂O₃; (B) 8.2 wt% K on γ-Al₂O₃; (C) 11.9 wt% K on γ-Al₂O₃.

tion of temperature. The TPD trace for native γ-Al₂O₃ has significant fine structure above 110°C associated with convoluted peaks representing NH₃ desorbing from surface acid sites of increasing strength. This fine structure is greatly diminished when the loading is increased to 8.2 and 11.9% potassium. For the 8.2% potassium sample, only weaker acid sites are interacting with the NH₃ below 400°C, and such sites desorb NH₃ very early in the temperature ramp. The 11.9% potassium sample again principally desorbs ammonia below 120°C. The sites associated with the second broad peak in the 11.9% potassium trace between 150 and 250°C may be an artifact of the synthesis protocol for this sample which required two impregnation and calcination steps, compared to the one required to make the 8.2% potassium sample. During the second impregnation, the surface may have been inadvertently rehydrated.

K-Doped Rh–Mo/γ-Al₂O₃

Again, the propensity of the surface of these materials to dehydrate MeOH is linked to the level of potassium loading on the samples. The microreactor results presented in Fig. 5 detail this trend for the K-doped Rh–Mo/γ-Al₂O₃ samples. Figure 5 contains data for samples synthesized by both the ion-exchange and aqueous-impregnation methods and demonstrates that as the potassium loading increases, the rate of formation of DME from MeOH diminishes. Most of the downward sloping trend in DME formation as a function of potassium loading is attributable to the first four points in this figure. These points represent the samples synthesized via the ion-exchange method and hence have lower potassium loadings. This section of Fig. 5 has an expanded x-axis scale which shows that for the sample with a 0.077%

Finally, as expected with γ-Al₂O₃, the concentration of acidic surface hydroxyls is insignificant as evidence by the lack of a strong signature Brønsted peak at ~1540 cm⁻¹.

The ammonia saturation and TPD results for the potassium-doped alumina samples are also consistent with the premise that increasing the potassium loading leads to decreased acidity. Table 1 lists the ammonia saturation results for selected catalyst samples synthesized for this study. As the first three entries of Table 1 indicate, the calculated number of reversible acid sites interacting with NH₃ below 400°C drops considerably for the 8.2 and 11.9% potassium samples compared to native γ-Al₂O₃. "Reversible sites" are defined here as those which desorb NH₃ during the heating cycle of the sample which includes a maximum temperature exposure of 400°C.

The reduction in acidity with increasing potassium loading is also demonstrated in Fig. 4, which depicts the TPD traces for the series of alumina samples as a func-
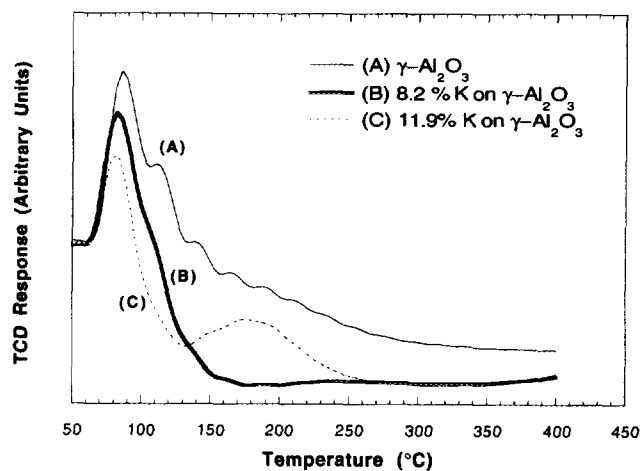

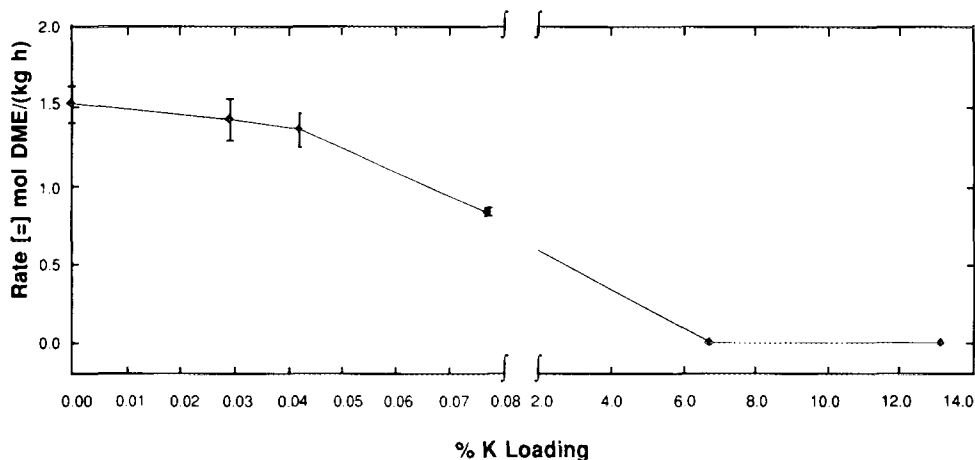FIG. 4. Ammonia temperature-programmed desorption for series of doped alumina samples.

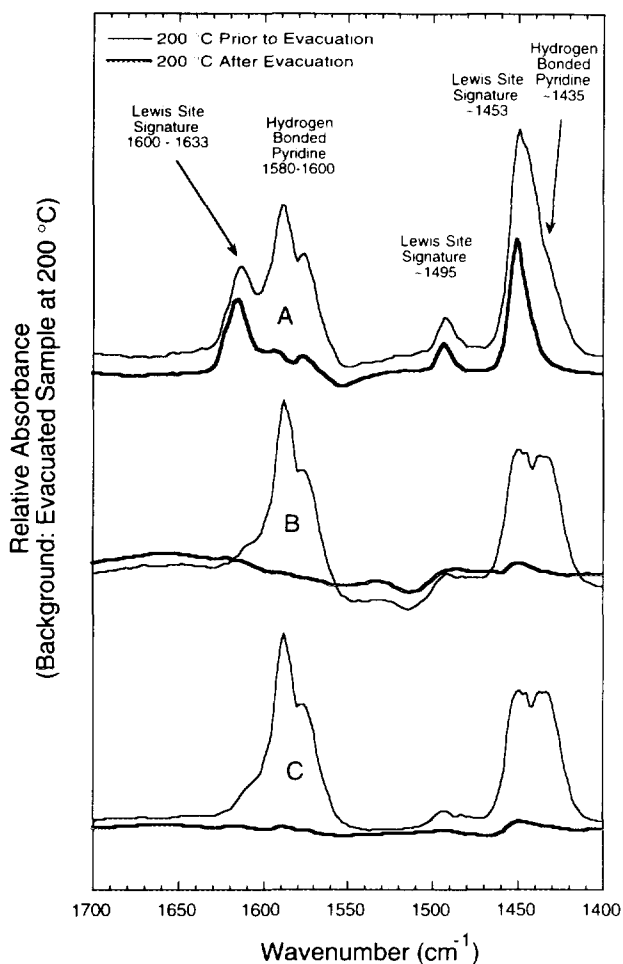FIG. 5.   Steady-state rate of dimethyl ether formation as a function of potassium loading on 2.8% Rh–3.4% Mo/γ-Al₂O₃.

FIG. 6.   IR spectra of adsorbed pyridine. (A) 2.5 wt% Mo/γ-Al₂O₃; (B) 2.8% Rh–3.4% Mo/γ-Al₂O₃; (C) 0.03% wt% K on 2.8% Rh–3.4% Mo/γ-Al₂O₃.

potassium loading, the rate of formation of DME has dropped by nearly a factor of 2 compared to the untreated Rh–Mo/γ-Al₂O₃ surface.

The pyridine adsorption spectra for the transition-metal-loaded samples are shown in Fig. 6. The spectral pair in Fig. 6A for Mo/γ-Al₂O₃ has essentially the same features as those in the spectral pair of Fig. 3A for native alumina, indicating the presence of significant Lewis acidity on the surface of this sample. In contrast, the spectral pair in Fig. 6B, the pyridine adsorption spectra for Rh–Mo/γ-Al₂O₃, has features reminiscent of a highly K-doped alumina. While Lewis acid signature peaks are present when the Rh–Mo/γ-Al₂O₃ sample is in equilibrium with pyridine vapor, these same peaks vanish when the sample is evacuated. Here, the process of chemisorbing the rhodium and oxidizing the catalyst has reduced the acidity of the surface. In Fig. 6C, which depicts the spectra for K-doped Rh–Mo/γ-Al₂O₃, the evacuated sample again lacks Lewis acid signature peaks. The spectrum for the evacuated, doped sample is essentially unchanged from that of the undoped sample (Fig. 6B, after evacuation).

Ammonia saturation and TPD results are presented in Table 1 and Figs. 7 and 8. The results presented in Table 1 and Fig. 7 indicate that the acid amount of sites interacting with NH₃ increases markedly upon addition of 2.5% molybdenum to the alumina surface. This increase can be related to the stoichiometry of the metals present on the surface, as will be discussed below. The TPD traces for the series of doped Rh–Mo/γ-Al₂O₃ samples (Fig. 8) suggest that while Table 1 indicates that the total acid amount of reversible sites may be unchanged, the distribution of reversible sites shifts toward sites which interact more strongly with ammonia after the surface has
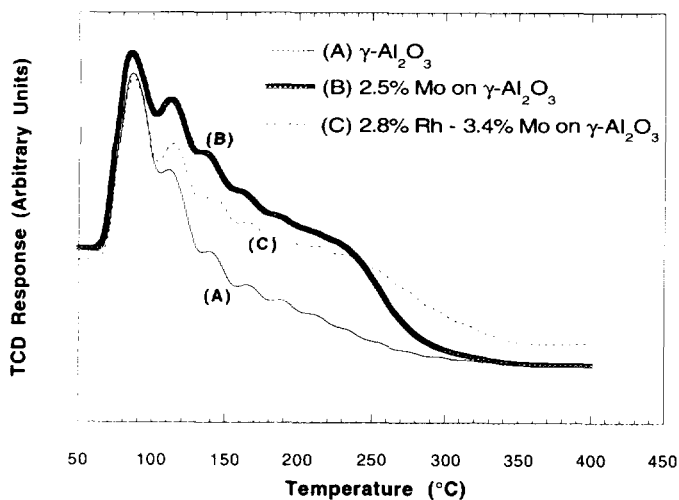
FIG. 7. Ammonia temperature-programmed desorption tracing acidity from native alumina to final bimetallic catalyst.

been doped with potassium. This effect, and its apparent contrast with the pyridine IR spectral analysis, may be associated with both (i) the ion-exchange protocol used to synthesize these samples which may have rehydrated the surface and (ii) the relative basicity of NH_3 compared to pyridine.

DISCUSSION

Past efforts to functionalize the alumina surface of rhodium-based catalysts focused on the role hydroxyl sites play in the sintering of monometallic, supported catalysts in high-temperature reactive environments. Yates and co-workers (15–17), in a series of investigations in 1991, demonstrated that in the presence of CO above 600 K, Rh(0) is oxidized on fully or patially hydroxylated alumina to form rhodium gem-dicarbonyl, $Rh(I)(CO)_2$, by the following surface reaction:

$$1/x \, RH_x^0 + Al{-}OH + 2 \, CO_{(g)} \rightarrow (Al{-}O^-)Rh^I(CO)_2$$
$$+ 1/2 \, H_{2(g)}.$$
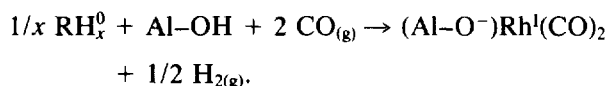
Yates and other researchers (18–21) contend that the formation of rhodium gem-dicarbonyl is correlated with rhodium's surface mobility and tendency to sinter and deactivate at high temperature. To combat this phenomenon, Yates first dehydroxylates the surface by evacuating Rh/γ-Al_2O_3 at high temperature (475–900 K) and later explores functionalizing the surface using both trimethyl silane and potassium (from K_2CO_3) to cap nucleophillic surface oxygen atoms and thus stabilize rhodium atoms in a highly dispersed array.

In contrast to the functionalization findings of Yates, the bimetallic materials synthesized in this study are thought to employ molybdenum, in the form of highly dispersed molybdenum anhydrides, to stabilize a high dispersion of rhodium. The efforts to potassium dope the surface of both the metal-loaded and native support are aimed, in part, at addressing the reactivity of the underlying alumina and stemming its retrograde dehydration activity. The approach is meant to synthesize an alkaline-metal oxide layer on the alumina surface which effectively screens primary alcohol products of hydrogenation from the adsorption sites of the support—believed here to be the Lewis acid–base pair sites. Our microreactor results demonstrate, as expected, that the potassium loading is directly correlated with dehydration activity for both native alumina and the Rh–Mo/γ-Al_2O_3. More intriguing, however, is the insight that can be drawn from this study about the nature of transition-metal chemisorption on the alumina surface during deposition from metal–carbonyl precursors.

Transition Metal Chemisorption Chemistry

The chemisorptive characterization of the samples with pyridine and ammonia supports our contention that the Lewis acid–base pairs play a key role in the dehydration mechanism, and the results are as expected for native alumina. The pyridine adsorption spectra in Fig. 6A indicate that after the chemisorption of Mo subcarbonyl on the alumina surface and the mild oxidation of this Mo/γ-Al_2O_3 sample, the surface acidity of the material is still significant. This result is in agreement with the work of Burwell and Brenner (22, 23), which suggests that
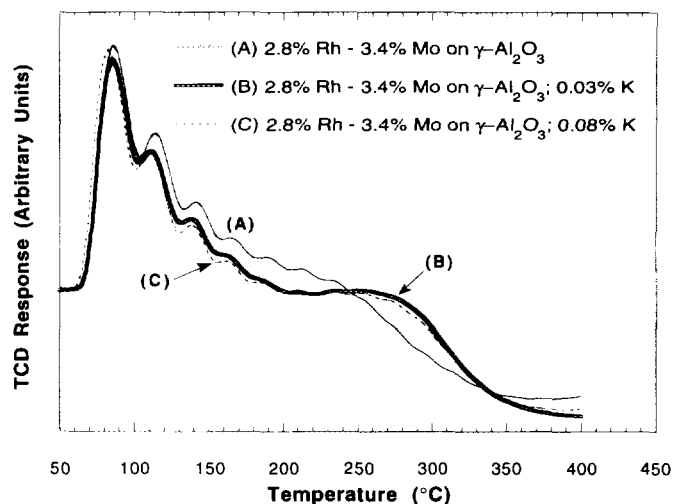

FIG. 8. Ammonia temperature programmed desorption for doped Rh–Mo/γ-Al_2O_3 series.

Mo(CO)₆ chemisorbs on alumina at hydroxyl sites rather than Lewis acid sites. If, upon oxidation of the material, the Mo subcarbonyl reacts with O_2 in the gas phase, the underlying Lewis acid sites of the support are left unmolested. The remaining Mo/γ-Al₂O₃ would have the acid sites associated with the underlying support and perhaps Lewis acid sites associated with the molybdenum anhydride centers on the surface. Hence the spectra in Fig. 6 indicate that considerable Lewis acidity is present on the surface of the 2.5% Mo/γ-Al₂O₃. Because the pyridine adsorptive technique is not quantitative, however, the increase in the acid amount, or number of pyridine-sensitive sites, cannot be accurately determined from the IR peak intensities given the degree of surface roughness in the self-supporting wafers used in this experiment.

Since the pyridine adsorption and IR analysis provided no quantitative measure of acid amount, we were motivated to use an adsorptive technique that could track the total amount of basic probe molecule adsorbed, namely, NH₃ saturation and TPD. Upon examination of the second column of Table 1, the total ammonia adsorption of the samples tested, a jump in total acidity of the surface is evident when the results for native alumina and Mo/γ-Al₂O₃ are compared. When the loading of Mo is increased from 2.5 to 3.4% in the 2.8% Rh–3.4% Mo sample, the total NH₃ capacity remains fairly constant. Essentially, the increase in Mo loading and, hence, the number of Lewis acid centers is offset by the interaction of Rh with the surface and its titration of some of the acid sites present.

The spectrum for the evacuated sample in Fig. 6 depicting the pyridine adsorption spectra for Rh–Mo/γ-Al₂O₃ (Fig. 6B, after evacuation) lacks Lewis signature peaks. This indicates that the process of chemisorbing the rhodium onto the Mo/γ-Al₂O₃ material diminishes or otherwise weakens the acid sites on Mo/γ-Al₂O₃. It is not surprising, then, that Fig. 6C looks indistinguishable, within experimental uncertainty, from Fig. 6B, after evacuation. The addition of potassium to the surface of Rh–Mo/γ-Al₂O₃ has no effect on the majority of acid sites sensitive to pyridine adsorption since these sites have already been weakened or eliminated by the presence of rhodium. This ameliorating effect of chemisorbed rhodium on the final acidic character of the Mo/γ-Al₂O₃ is also the key to (i) interpreting the microreactor results of Fig. 5 and (ii) the observation in the synthesis of the materials that the ultimate potassium loading achievable on Rh–Mo/γ-Al₂O₃ using the ion-exchange method is only a fraction of that for native alumina (as high as 3%) when both are exposed to the same concentration of KNO₃. The majority of the acidic character typically available for MeOH dehydration and available to interact with potassium cations has already been eliminated by chemisorbing rhodium.

The relation between the transition-metal loading and the acidity of the surface of the materials in this study can be tracked in a self-consistent fashion. On native alumina, the ammonia saturation data in Table 1 suggests that the amount of ammonia-adsorbing sites is approximately 2450 μmoles/g. In Peri's model for the surface of dehyrated γ-Al₂O₃ (24), the hydroxyl site density is approximately 8 to 12 hyroxyl sites per 100 Å². If we assume that (i) the MoOₓ is present as the surface molybdate Mo(VI)O₄ (see Fig. 9), as XPS analysis indicates (1) and Raman spectroscopic investigations by Stencel et al. (25) and Wachs and co-workers (26–29) suggest, (ii) the Mo has interacted with two hydroxyl sites per atom of Mo in chemisorbing and oxidatively binding to the surface, and (iii) each Mo center acts as a Lewis acid site in the presence of NH₃ which can adsorb two NH₃ molecules per Mo, then the stoichiometry on the 2.5% Mo/γ-Al₂O₃ sample suggests that it should adsorb approximately 2910 μmoles/g of NH₃. This simple calculated value deviates by only 3% from the experimentally measured NH₃ capacity on the 2.5% Mo/γ/Al₂O₃, as reported in Table 1. In proceeding to consider the expected acid character of the 2.8% Rh–3.4% Mo/γ-Al₂O₃, an adjustment must be made for the increase in Mo loading. Considering first only the influence of the Mo, based on the assumptions above, the 2.8% Rh–3.4% Mo sample would be expected to adsorb approximately 3010 μmoles/g. If (i) the Rh present on the surface after oxidation of the catalyst is present as Rh(III), as XPS analysis indicates (1), (ii) the rhodium oxide screens three Lewis acid sites of the support per Rh atom, and (iii) each Rh atom is again capable of adsorbing two NH₃ molecules, then the implied stoichiometry suggests that the 2.8% Rh–3.4% Mo/γ-Al₂O₃ should have an NH₃ capacity of 2738 μmoles/g. This value accounts for 96% of the NH₃ capacity measured experimentally. These calculations provide a systematic basis for interpreting the experimental observation that the presence of the Rh diminishes at least part of the acidity present on Mo/γ-Al₂O₃.

The final issue which must be addressed in considering the adsorptive behavior of the transition-metal-loaded samples considered in this study concerns the difference in their adsorptive behavior in the presence of ammonia versus pyridine. The evacuated pyridine IR spectrum in
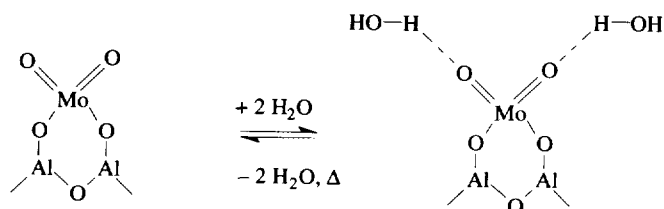

FIG. 9. Mo(VI)O₄ surface species adapted from Ref. (25).

Fig. 6 for the Rh–Mo/γ-Al$_2$O$_3$ sample was similar to that of highly potassium-doped native alumina, yet the NH$_3$ saturation data of Table 1 suggest that the acid amount of the Rh–Mo sample is considerably larger than that of, say, doped 8.2% K on alumina sample. First, the pyridine adsorption study provided no quantitative measure of acid amount—technically, the acid *strength* of the Rh–Mo sample is comparable to that of highly doped alumina as measured by pyridine adsorption. Second, the relative tendency of NH$_3$ and pyridine to coordinate with transition-metal centers is strongly dependent on the π*-back-bonding ability, and hence, the oxidation state, of the transition-metal center. Shepherd and Taube (30) have calculated *the relative ligand exchange rates for* NH$_3$ and pyridine with [(NH$_3$)$_5$RuOH$_2$]$^{2+}$ and [(NH$_3$)$_5$RuOH$_2$]$^{3+}$, wherein the H$_2$O coordination site was replaced. In their study, Shepherd and Taube calculate that for Ru^{2+}, the affinity ratio of pyridine to NH$_3$ was approximately 2 : 1, and the greater affinity for pyridine resulted from the ~5.8 kcal/mol relative contribution to the free energy of association due to backbonding to the pyridine. In contrast, for the Ru^{3+} which was assumed to have no net backbonding to the pyridine, the pyridine to NH$_3$ affinity ratio was approximately 1 : 4 (1 : 24 after accounting for a statistical factor of six in the case of NH$_3$). In this study, the molybdenum and rhodium—like the Ru^{3+} of Shepherd and Taube's work—are present in a highly oxidized state prior to reduction. Hence, sites sensitive to strong NH$_3$ adsorption on the Rh–Mo and Mo on γ-Al$_2$O$_3$ surface may not bond as strongly to pyridine, and the adsorption results for NH$_3$ and pyridine should be expected to quantitatively differ.

CONCLUSIONS

The results presented for the series of K-doped alumina and Rh–Mo/γ-Al$_2$O$_3$ samples synthesized in this study demonstrate that the MeOH dehydration propensity of these materials can be quantified and manipulated. This dehydration propensity has been correlated to the strength and amount of Lewis acid sites on the surface through analysis of the IR spectra of adsorbed pyridine and the NH$_3$ saturation and TPD data. The IR spectra of adsorbed pyridine and the NH$_3$ saturation and TPD data on the Rh–Mo/γ-Al$_2$O$_3$ samples show that addition of rhodium diminishes surface acidity of Mo/γ-Al$_2$O$_3$. This amelioration of acidity is evidenced by the observation that less than 6 wt% potassium doping is required on the Rh–Mo catlyst to completely eliminate the DME activity compared to more than 12 wt% on native γ-Al$_2$O$_3$ at temperatures of up to 250°C. Furthermore, the chemisorptive characterization of the transition-metal-loaded samples synthesized in this investigation is consistent with the contention of Burwell and Brenner (22, 23) that the

Mo(CO)$_6$ interacts primarily with hydroxyl sites on the surface of the alumina. While the chemisorbing molybdenum subcarbonyls may not materially alter the Lewis acidity of the underlying support, such adsorbed and oxidized molybdenum centers seem to function as Lewis acid sites in the presence of NH$_3$. The Lewis acid character of the Mo centers is suggested by the dramatic jump in NH$_3$ capacity upon addition of Mo to the alumina surface. The process of chemisorbing and oxidizing a second, active transition metal from Rh(I)(CO)$_2$(*acac*) leads to a dramatic reduction in the strength of the Lewis acid sites on the surface and diminishes the number of sites which actively adsorb NH$_3$. Additional chemisorptive characterization of transition-metal-loaded samples is underway, and such studies are hoped to add more conclusive evidence to the stoichiometric arguments presented under Discussion herein.

ACKNOWLEDGMENTS

REFERENCES

1. Foley, H. C., Hong, A. J., Brinen, J. S., Allard, L. F., and Garratt-Reed, A. J., *Appl. Catal.* **61**, 351 (1990).
2. Te, M., Lowenthal, E. E., and Foley, H. C., *J. Catal.* **146**, 591 (1994).
3. Kip, B. J., Hermans, E. G. F., van Wolput, J. H. M. C., Hermans, N. M. A., van Grondelle, J., and Prins, R., *Appl. Catal.* **35**, 109 (1987).
4. Trunschke, A., Ewald, H., Gutschick, D., Miessner, H., Skupin, M., Walther, B., and Böttcher, H.-C., *J. Mol. Catal.* **56**, 95 (1989).
5. Trunschke, A., Ewald, H., Miessner, H., Fukuoka, A., Ichikawa, M., and Böttcher, H.-C., *Mater. Chem. Phys.* **29**, 503 (1991).
6. Trunschke, A., Ewald, H., Miessner, H., Marengo, S., Martinengo, S., Pinna, F., and Zanderighi, L., *J. Mol. Catal.* **74**, 365 (1992).
7. Wardinsky, M. D., and Hecker, W. C., *J. Phys. Chem.* **92**, 2602 (1988).
8. Decanio, E. C., and Storm, D. A., *J. Catal.* **132**, 375 (1991).
9. Jain, J. R., and Pillai, C. N., *J. Catal.* **9**, 322 (1967).
10. Parera, J. M., and Figoli, N. S., *J. Catal.* **14**, 303 (1969).
11. Padmanabhan, V. R., and Eastburn, F. J., *J. Catal.* **24**, 88 (1972).
12. Knözinger, H., Kochloefl, K., and Meye, W., *J. Catal.* **28**, 69 (1973).
13. Decanio, E. C., Nero, V. P., and Bruno, J. W., *J. Catal.* **135**, 444 (1992).
14. Parry, E. P., *J. Catal.* **2**, 371 (1963).
15. Ballinger, T. H., and Yates, J. T., Jr., *J. Phys. Chem.* **95**, 1694 (1991).
16. Paul, D. K., and Yates, J. T., Jr., *J. Phys. Chem.* **95**, 1699 (1991).
17. Zaki, M. I., Ballinger, T. H., and Yates, J. T., Jr., *J. Phys. Chem.* **95**, 4028 (1991).
18. Solymosi, F., and Pásztor, M., *J. Phys. Chem.* **89**, 4789 (1985).
19. Solymosi, F., and Pásztor, M., *J. Phys. Chem.* **90**, 5312 (1986).

20. Zaki, M. I., Kunzmann, G., Gates, B. C., and Knözinger, H., *J. Phys. Chem.* **91**, 1486 (1987).
21. Wong, C., and McCabe, R. W., *J. Catal.* **119**, 47 (1989).
22. Brenner, A., and Burwell, R. L., Jr., *J. Catal.* **52**, 353 (1978).
23. Burwell, R. L., and Brenner, A., *J. Mol. Catal.* **1**, 77 (1975).
24. Peri, J. B., *J. Phys. Chem.* **69**, 231 (1965).
25. Stencel, J. M., Makovsky, L. E., Sarkus, T. A., De Vries, J., Thomas, R., and Moulin, J. A., *J. Catal.* **90**, 314 (1984).
26. Chan, S. S., Wachs, I. E., Murrell, L. L., Wang, L., and Hall, W. K., *J. Phys. Chem.* **88**, 5831 (1984).
27. Hardcastle, F. D., and Wachs, I. E., *J. Raman Spectrosc.* **21**, 683 (1990).
28. Williams, C. C., Ekerdt, J. G., Jehng, J.-M., Hardcastle, F. D., and Wachs, I. E., *J. Phys. Chem.* **95**, 8791 (1991).
29. Vuurman, M. A., and Wachs, I. E., *J. Phys. Chem.* **96**, 5008 (1992).
30. Shepherd, R. E., and Taube, H., *Inorg. Chem.* **12**, 1392 (1973).